TITLE: Sampling the conformational landscapes of transporters and receptors with AlphaFold2

AUTHORS: Diego del Alamo* (1,2), Davide Sala* (3), Hassane S. Mchaourab† (1), Jens Meiler† (2,3)
1. Department of Molecular Physiology and Biophysics, Vanderbilt University, Nashville, TN, USA
2. Department of Chemistry, Vanderbilt University, Nashville, TN, USA
3. Institute for Drug Discovery, Leipzig University, Leipzig, DE

* Equal contribution
† Correspondence: hassane.mchaourab@vanderbilt.edu, jens@meilerlab.org

ABSTRACT

Equilibrium fluctuations and triggered conformational changes often underlie the functional cycles of membrane proteins. For example, transporters mediate the passage of molecules across cell membranes by alternating between inward-facing (IF) and outward-facing (OF) states, while receptors undergo intracellular structural rearrangements that initiate signaling cascades. Although the conformational plasticity of these proteins has historically posed a challenge for traditional *de novo* protein structure prediction pipelines, the recent success of AlphaFold2 (AF2) in CASP14 culminated in the modeling of a transporter in multiple conformations to high accuracy. Given that AF2 was designed to predict static structures of proteins, it remains unclear if this result represents an underexplored capability to accurately predict multiple conformations and/or structural heterogeneity. Here, we present an approach to drive AF2 to sample alternative conformations of topologically diverse transporters and G-protein coupled receptors (GPCRs) that are absent from the AF2 training set. Whereas models generated using the default AF2 pipeline are conformationally homogeneous and nearly identical to one another, reducing the depth of the input multiple sequence alignments (MSAs) led to the generation of accurate models in multiple conformations. In our benchmark, these conformations were observed to span the range between two experimental structures of interest, suggesting that our protocol allows sampling of the conformational landscape at the energy minimum. Nevertheless, our results also highlight the need for the next generation of deep learning algorithms to be designed to predict ensembles of biophysically relevant states.

INTRODUCTION

Dynamic interconversion between multiple conformations drive the functions of integral membrane proteins in all domains of life[1–4]. For example, the vectorial translocation of substrates by transporters is mediated by movements that open and close extracellular and intracellular gates[5,6]. For GPCRs, ligand binding on the extracellular side triggers structural rearrangements on the intracellular side that initiate downstream signaling[7,8]. Traditional computational prediction pipelines reliant on inter-residue distance restraints calculated from deep MSAs have historically struggled to accurately predict the structures of these proteins and their movements. The resultant models are unnaturally compact and frequently distorted, preventing critical questions about ligand and/or drug binding modes from being addressed[9,10].

A performance breakthrough was unveiled during CASP14 by AF2[11–15], which achieved remarkably accurate *de novo* structure prediction. Upon examining the list of CASP14 targets and

corresponding models, we found that AF2 modeled the multidrug transporter LmrP (target T1024) in multiple conformations, each of which was individually consistent with published experimental data[16–20]. This exciting observation stimulated the question of whether such performance can be duplicated for other membrane proteins. At its essence, this question centers on whether AF2 can sample the conformational landscape in the minimum energy basin. Here, we investigate this question using a benchmark set of topologically diverse transporters and GPCRs. Our results demonstrate that reducing the depth of the input MSAs is conducive to the generation of accurate models in multiple conformations by AF2, suggesting that the algorithm's outstanding predictive performance can be extended to sample alternative structures of the same target. For most proteins considered, we report a striking correlation between the breadth of structures predicted by AF2 and the ground truth as observed by cryo-EM and/or X-ray crystallography. Finally, we propose a modeling pipeline for researchers interested in obtaining two distinct conformations of a membrane protein and apply it to the structurally unknown GPR114/AGRG5 adhesion GPCR as an example.

RESULTS AND DISCUSSION

By necessity, this study is restricted to proteins whose structures 1) are determined at atomic resolution in two or more conformations and 2) are entirely absent from the AF2 training set. We selected five transporters that not only met these criteria but also reflect a range of transport mechanisms characterized in the literature[5], including rocking-bundle (Lat1[21,22], ZnT8[23]), rocker-switch (MCT1[24], STP10[25]), and elevator (ASCT2[26,27]) mechanisms of transport (Figure S1 and Table S1). We also included three GPCRs, which were distributed across classes A (CGRPR[28,29]), B1 (PTH1R[30,31]), and F (FZD7[32]; to serve as points of comparison, we used the active conformation of FZD7 and the inactive conformation of the nearly identical FZD4[33]).

AF2 generates multiple conformations of all eight target proteins

The sequences of all targets were truncated to remove large soluble and/or intrinsically disordered regions which represent a challenge for AF2. The structures were then predicted using the default AF2 structure prediction pipeline in the absence of templates[12]. However, the resulting models were largely identical to one another and failed to shed light on the target protein's conformational space. We therefore diversified the models generated by AF2 by disabling recycling, which limited the algorithm to a single pass, and by providing MSAs of varying depths including as few as 32 sequences (see *Methods*). To sample the conformational landscape more exhaustively, we generated fifty models of each protein for each MSA size, while eliminating postprocessing with OpenMM[34] to reduce the pipeline's total computational cost. For the targets, each model's similarity to the experimental OF and IF structures was quantified using TM-score[35–37], a metric which indicates how well the two structures superimpose over one another, with scores ranging from 0 (arbitrarily different) to 1 (perfect overlap; Figure 1A).

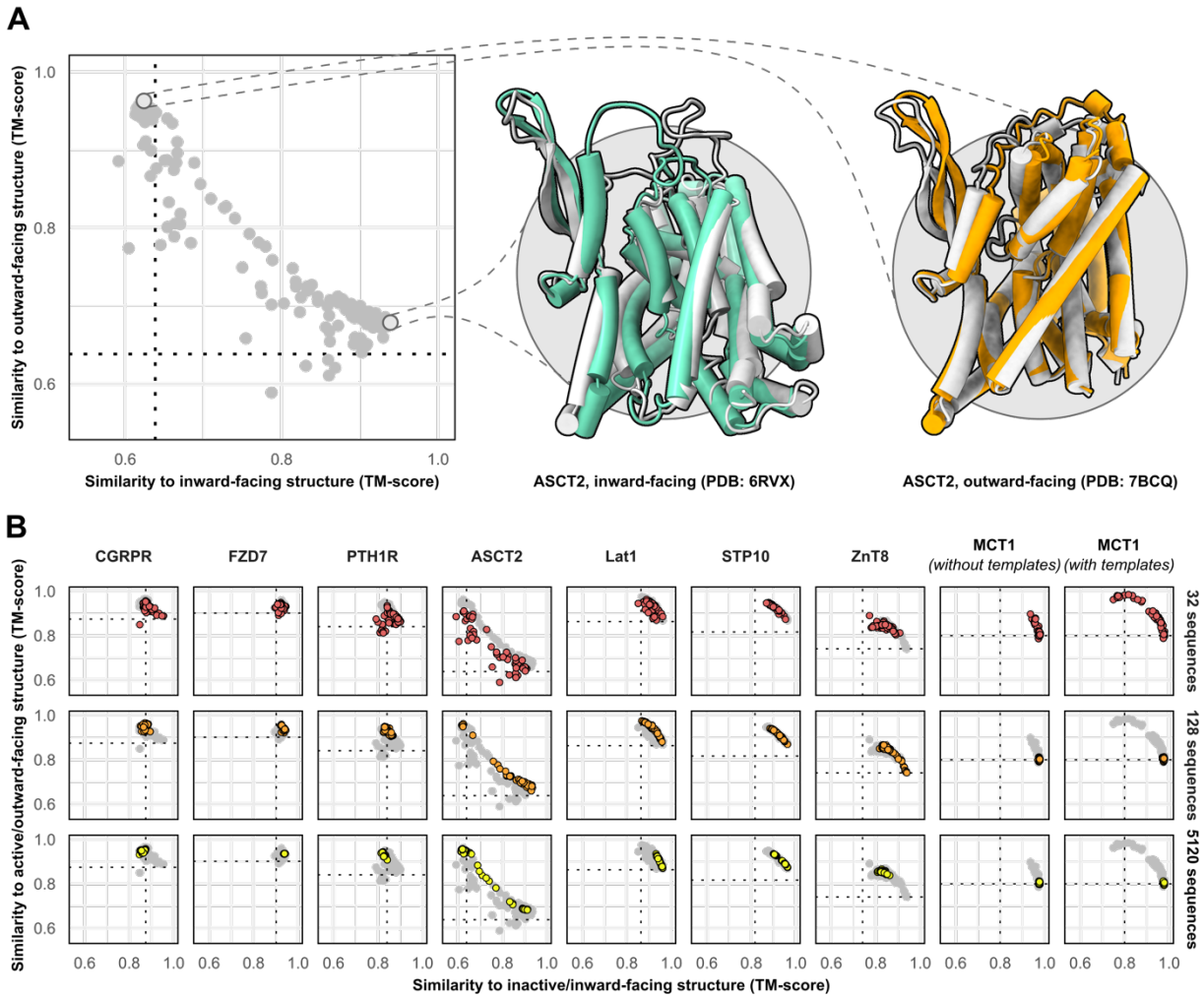

Figure 1. Alternative conformations of transporters and GPCRs can be predicted by AF2. (A) Representative models of the transporter ASCT2 in IF and OF conformations. Experimental structures shown in colors and models shown in gray. **(B)** Comparison of each model with both experimental structures as a function of MSA depth. Each colored point represents one of fifty models generated for a given MSA size, with points in gray shared across all MSA sizes for reference. Models of all proteins except MCT1 were generated without templates. For prediction of MCT1 with templates, only outward-facing structures of homologs were provided. Dashed lines indicate the TM-score between experimental structures and are shown for reference.

Accurate models of all eight protein targets were obtained for at least one conformation, consistent with published performance statistics[12] (Figure 1B). Whereas larger MSAs were observed to engender tighter clustering in specific conformations, MSAs consisting of just 32 sequences appeared to promote the generation of alternative conformations in seven benchmark proteins. This diversity coincided with generation of misfolded models in several cases, particularly of ASCT2 and Lat1, the two largest proteins in our dataset (example model shown in Figure S2). Unlike the models of interest that overlapped with ground truth experimental structures, however, misfolded models virtually never co-clustered and could thus be easily identified and excluded from further analysis[38]. While padding MSAs with additional sequences had the desirable effect of decreasing the proportion of these models, it also limited the extent to

which alternative conformations were sampled. Thus, our results revealed a delicate balance that must be achieved to generate models that are both diverse and natively folded. No general pattern was readily apparent regarding the ideal MSA depth required to achieve this balance.

One target, MCT1, was exclusively modeled by AF2 in either IF or fully occluded conformations regardless of MSA depth. Notably, these results closely parallel those reported by DeepMind during their attempt to model multiple conformations of LmrP in CASP14[17]. We therefore adapted their approach by providing templates of homologs in exclusively OF conformations alongside MSAs of various sizes and obtained several accurate OF models only when shallow MSAs were provided (32 sequences). Nevertheless, OF models constituted a minor population in an ensemble dominated by occluded or IF models. Thus, the generation of large numbers of models appeared to be necessary to yield intermediate conformations of interest. Similar results were observed when we modeled PTH1R using either exclusively inactive or active templates, as well as Lat1 using either exclusively OF or IF templates (Figure S3), further indicating that the information content provided by the templates diminishes as the depth of the MSA increases.

Overall, these results demonstrate that highly accurate models adopting both conformations of all eight protein targets could be predicted with AF2 by using MSAs that are far shallower than the default. However, because the optimal MSA depth and choice of templates varied for each protein, they also argue against a one-size-fits-all approach for conformational sampling.

Predicted conformational fluctuations correlate with implied conformational dynamics

To further investigate the structural heterogeneity predicted by these models, we computed each residue's root mean squared deviation (RMSD) between the two experimental structures, as well as their root mean squared fluctuation (RMSF) values among all fifty models following structure-based alignment (Figure 2). Correlation between these two measures were observed in most cases and was notable for ASCT2, Lat1, CGRPR, and MCT1 with templates ($R^2 \geq 0.75$). The exception was MCT1 without templates, which was likely due to a lack of conformational diversity among the sampled models. The inclusion of templates restored this correlation in MCT1 but contributed negligibly to those of PTH1R and Lat1 (Figure S4). The correlation demonstrates that predicted flexibility by AF2 is related to the protein's dynamics implied from the experimental structures. In contrast with a recent preprint[39], the predicted flexibility values failed to correlate with the predicted confidence metric pLDDT[40].

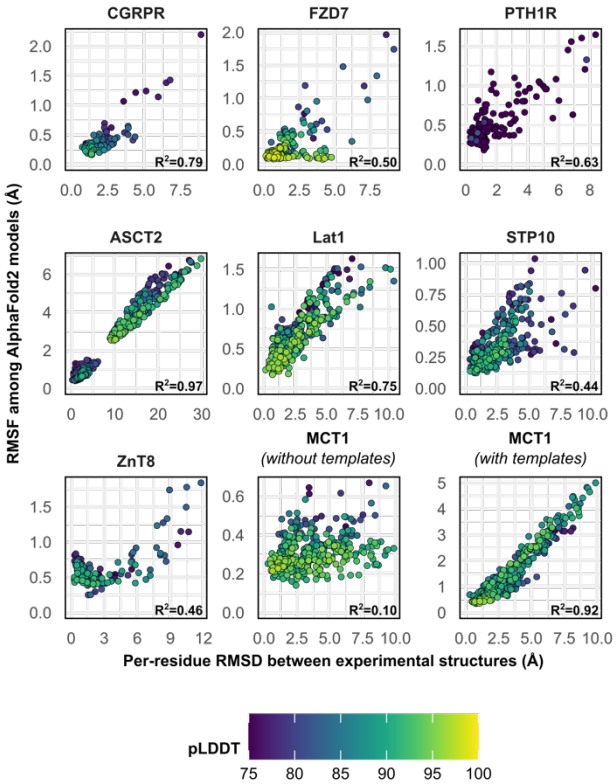

Figure 2. Correlation between residue implied movement in the experimental structures and its variability in AF2 models. Residues with low confidence (pLDDT≤75) were omitted from this plot for all proteins except PTH1R. MSA sizes of 128 sequences were used for all predictions, except for MCT1 with templates, which instead used 32 sequences to capture the OF conformation. pLDDT refers to each residue's predicted accuracy, with a value of 100 indicating maximum confidence.

<u>Distributions of predicted models relative to the experimental structures</u>

Visual examination suggested that many of the predicted models fall "in between" the two experimentally determined conformations (example shown in Figure 3A). Furthermore, certain structural features expected to be conformationally heterogeneous, such as long loops, appeared to be nearly identical across these models. Both observations raised questions about the relationship between the diversity of the predicted models and the breadth of the conformational ensembles bracketed by the experimental structures. To quantitatively place the predicted conformational variance in the context of the ground truth structures, we used principal component analysis (PCA), which reduces the multidimensional space to a smaller space representative of the main conformational motions. In our benchmark set, the first principal component (PC1) captured 64.9±16.1% of the structural variations among the models (Figure 3). The experimental structures virtually always occupied well defined extreme positions. In every case, an unexpected correlation was evident between each model's PC1 values and their TM-scores (Figure 3B). Indeed, the models with the most extreme PC1 values were also among the most accurate, and the experimental structure virtually always flanked the AF2 models along PC1. The exception, PTH1R, was determined in a partially inactive and active conformation[30], suggesting that models

extending beyond the former state along PC1 may represent the fully inactive conformation. This may suggest that distinct conformers can be modeled and identified simply by selecting the extreme positions along PC1.

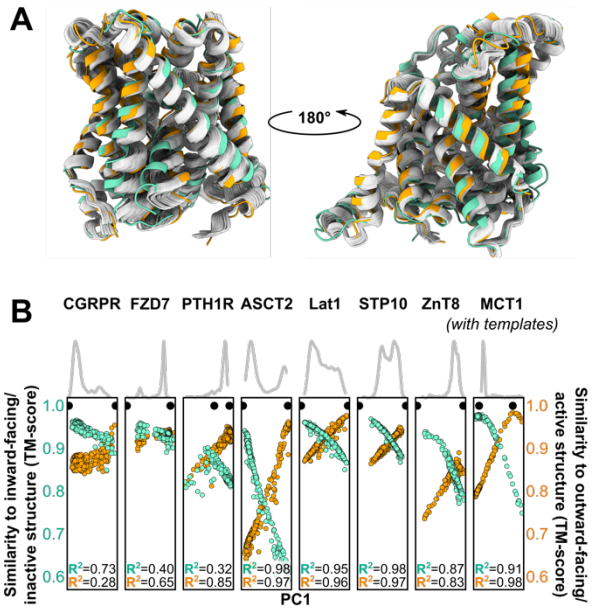

Figure 3. Distinct conformations can be delineated using PCA. (A) Conformational heterogeneity in AF2 models of **Lat1.** Experimental IF and OF conformations shown in teal and orange, respectively, while representative AF2 models shown in white. **(B)** Distribution of AF2 models across the first principal component (PC1) following PCA (gray traces). Scatter plots comparing each model's position along PC1 and its structural similarity to ground truth structures. Teal: Similarity to IF (transporters) or inactive (GPCRs) conformation. Orange: Similarity to OF (transporters) or active (GPCRs) conformation. Each model is shown twice, once in teal and once in orange. Native structures are shown as black dots.

<u>Alternative conformations cannot be predicted for proteins with structures in the training set</u>

A necessary follow-up question centers on whether this strategy can yield similar results for proteins with one conformation present in the AF2 training set. We investigated this question using four membrane proteins with two experimentally determined conformations, at least one of which was included in the AF2 training set: the class A GPCR CCR5[41,42], the serotonin transporter SERT[43,44], the multidrug transporter PfMATE[45,46], and the lipid flippase MurJ[47,48] (Table S2). Using the template-free prediction pipeline outlined above, we then monitored the resultant models' similarity to the structures included in and absent from the training set. Unlike the results presented above, virtually every transporter model superimposed nearly perfectly with the training set conformation, and none resembled the alternative conformation (Figure S5). The conformational diversity of these models, including those generated using shallow MSAs, was far more limited than what was observed for the five proteins discussed above. Indeed, observed conformational diversity was limited to a handful of occluded models of MurJ and PfMATE but none of the models observed adopted the alternative conformer. By contrast, while models of CCR5 were less biased toward the training set conformation, deep MSAs reduced conformational diversity. This

divergence in performance may stem from the composition of the AF2 training set, which featured the structures of many active GPCRs but no structures, for example, of inward-facing MATEs[49].

Concluding remarks: proposed workflow and future directions

Our results indicate that the state-of-the-art *de novo* structural modeling algorithm AF2 can be manipulated to accurately model alternative conformations of transporters and GPCRs whose structures were not provided during training. The use of shallow MSAs was instrumental to obtaining structurally diverse models, and in one case (MCT1) accurate modeling of alternative conformations also required the manual curation of template models. Thus, there is no one-size-fits-all approach for sampling conformational space with high accuracy. Indeed, whereas the DeepMind team reportedly required templates to obtain models of LmrP in an OF conformation[17], we found that this procedure was usually unnecessary. Accurate representatives of distinct conformers were generally obtainable with exhaustive sampling and could be identified by performing PCA and selecting models at or near the extreme positions of PC1. Nevertheless, prediction pipelines will likely require fine-tuning specific to each target of interest followed by experimental verification of proposed conformers. Moreover, this approach does not appear to extend to proteins whose structures were provided during training, hinting at the possibility that traditional methods may still be required to capture alternative conformers[50,51].

As a final verification of this proposed pipeline, we tested it on GPR114/AGRG5, a class B2 adhesion GPCR whose structure has not been experimentally determined. The structural model deposited in the AF2 database, which likely depicts an active conformation that diverges from the structure of the homolog GPR97[52], could be recapitulated by using deep MSAs. The use of shallow MSAs (≤64 sequences), by contrast, yielded a range of intermediate conformations distributed across three well-separated clusters (Figure S6). One of these clusters, shown in pink in Figure S6B, contains models with an orientation of TM6 and TM7 that fully occludes the orthosteric site and partially blocks the cytosolic pocket where G-proteins putatively bind.

While these results reinforce the notion that AF2 can provide models to guide biophysical studies of conformationally heterogeneous membrane proteins, they represent a methodological "hack", rather than an explicit objective built into the algorithm's architecture. Several preprints have provided evidence that AF2, despite its accuracy, likely does not learn the energy landscapes underpinning protein folding and function[39,53,54]. We believe that our results bolster these findings and highlight the need for further development of artificial intelligence methods capable of learning the conformational flexibility intrinsic to protein structures.

METHODS

Prediction runs were executed using AlphaFold v2.0.1 and a modified version of ColabFold[55] that is available for download at www.github.com/delalamo/af2_conformations. MSAs were obtained using the MMSeqs2 server[56,57], and specific MSA sizes were used by modifying the "max_msa_clusters" and "max_extra_msa" parameters prior to execution. Throughout this manuscript, the latter corresponds to the depth of the MSA, and "max_msa_clusters" was set to either 16 (when using MSAs with 32 sequences), 64 (128 sequences), or 512 (5120 sequences). When templates were used to model MCT1, they were chosen by manual inspection, and the parameter "subsample_templates" was set to *True*. All structure-based alignments and TM-score calculations were carried out using TM-align[37]. Principal

component analysis was carried out using CPPTRAJ[58]. Figures were made with ChimeraX[59] and ggplot2[60].

REFERENCES

1. Cournia, Z. *et al*. Membrane Protein Structure, Function, and Dynamics: a Perspective from Experiments and Theory. *J. Membr. Biol*. **248**, 611–640 (2015).
2. Campbell, E. *et al*. The role of protein dynamics in the evolution of new enzyme function. *Nat. Chem. Biol*. **12**, 944–950 (2016).
3. Shaw, D. E. *et al*. Atomic-level characterization of the structural dynamics of proteins. *Science (80-.)*. **330**, 341–346 (2010).
4. Boehr, D. D., Nussinov, R. & Wright, P. E. The role of dynamic conformational ensembles in biomolecular recognition. *Nature Chemical Biology* vol. 5 789–796 (2009).
5. Boudker, O. & Verdon, G. Structural perspectives on secondary active transporters. *Trends Pharmacol. Sci*. **31**, 418–426 (2010).
6. Kazmier, K., Claxton, D. P. & Mchaourab, H. S. Alternating access mechanisms of LeuT-fold transporters: trailblazing towards the promised energy landscapes. *Curr. Opin. Struct. Biol*. **45**, 100–108 (2017).
7. Wang, J., Hua, T. & Liu, Z. J. Structural features of activated GPCR signaling complexes. *Curr. Opin. Struct. Biol*. **63**, 82–89 (2020).
8. Gusach, A. *et al*. Beyond structure: emerging approaches to study GPCR dynamics. *Curr. Opin. Struct. Biol*. **63**, 18–25 (2020).
9. Ovchinnikov, S. *et al*. Large-scale determination of previously unsolved protein structures using evolutionary information. *Elife* **4**, 1–25 (2015).
10. Nicoludis, J. M. & Gaudet, R. Applications of sequence coevolution in membrane protein biochemistry. *Biochim. Biophys. Acta - Biomembr*. **1860**, 895–908 (2018).
11. Jumper, J. & Evans, R. High Accuracy Protein Structure Prediction Using Deep Learning. in *Fourteenth Critical Assessment of Techniques for Protein Structure Prediction (Abstract Book)* 22–24 (2020).
12. Jumper, J. *et al*. Highly accurate protein structure prediction with AlphaFold. *Nature* (2021) doi:10.1038/s41586-021-03819-2.
13. Tunyasuvunakool, K. *et al*. Highly accurate protein structure prediction for the human proteome. *Nature* (2021) doi:10.1038/s41586-021-03828-1.
14. Pereira, J. *et al*. High-accuracy protein structure prediction in CASP14. *Proteins Struct. Funct. Bioinforma*. 1–13 (2021) doi:10.1002/prot.26171.
15. Alexander, L. T. *et al*. Target highlights in CASP14: Analysis of models by structure providers. *Proteins Struct. Funct. Bioinforma*. 1–26 (2021) doi:10.1002/prot.26247.
16. del Alamo, D., Govaerts, C. & Mchaourab, H. S. AlphaFold2 predicts the inward-facing conformation of the multidrug transporter LmrP. *Proteins Struct. Funct. Bioinforma*. 10–12 (2021) doi:10.1002/prot.26138.
17. Jumper, J. *et al*. Applying and improving AlphaFold at CASP14 . *Proteins Struct. Funct. Bioinforma*. (2021) doi:10.1002/prot.26257.
18. Debruycker, V. *et al*. An embedded lipid in the multidrug transporter LmrP suggests a mechanism for polyspecificity. *Nat. Struct. Mol. Biol*. **27**, 829–835 (2020).
19. Masureel, M. *et al*. Protonation drives the conformational switch in the multidrug transporter LmrP. *Nat. Chem. Biol*. **10**, 149–155 (2014).
20. Martens, C. *et al*. Lipids modulate the conformational dynamics of a secondary multidrug transporter. *Nat. Struct. Mol. Biol*. **23**, 744–751 (2016).
21. Yan, R., Zhao, X., Lei, J. & Zhou, Q. Structure of the human LAT1–4F2hc heteromeric

amino acid transporter complex. *Nature* **568**, 127–130 (2019).
22. Yan, R. *et al*. Mechanism of substrate transport and inhibition of the human LAT1-4F2hc amino acid transporter. *Cell Discov*. **7**, (2021).
23. Xue, J., Xie, T., Zeng, W., Jiang, Y. & Bai, X. C. Cryo-EM structures of human ZnT8 in both outward-and inward-facing conformations. *Elife* **9**, 1–32 (2020).
24. Wang, N. *et al*. Structural basis of human monocarboxylate transporter 1 inhibition by anti-cancer drug candidates. *Cell* **184**, 370-383.e13 (2021).
25. Bavnhøj, L., Paulsen, P. A., Flores-Canales, J. C., Schiøtt, B. & Pedersen, B. P. Molecular mechanism of sugar transport in plants unveiled by structures of glucose/H+ symporter STP10. *Nat. Plants* **7**, 1409–1419 (2021).
26. Garibsingh, R. A. A. *et al*. Rational design of ASCT2 inhibitors using an integrated experimental-computational approach. *Proc. Natl. Acad. Sci. U. S. A.* **118**, (2021).
27. Garaeva, A. A., Guskov, A., Slotboom, D. J. & Paulino, C. A one-gate elevator mechanism for the human neutral amino acid transporter ASCT2. *Nat. Commun*. **10**, 1–8 (2019).
28. Liang, Y.-L. *et al*. Structure and Dynamics of Adrenomedullin Receptors AM1 and AM2 Reveal Key Mechanisms in the Control of Receptor Phenotype by Receptor Activity-Modifying Proteins. *ACS Pharmacol. Transl. Sci*. **3**, 263–284 (2020).
29. Josephs, T. M. *et al*. Structure and dynamics of the CGRP receptor in apo and peptide-bound forms. *Science (80-.)*. **372**, eabf7258 (2021).
30. Ehrenmann, J. *et al*. High-resolution crystal structure of parathyroid hormone 1 receptor in complex with a peptide agonist. *Nat. Struct. Mol. Biol*. **25**, 1086–1092 (2018).
31. Zhao, L.-H. *et al*. Structure and dynamics of the active human parathyroid hormone receptor-1. *Science (80-.)*. **364**, 148–153 (2019).
32. Xu, L. *et al*. Cryo-EM structure of constitutively active human Frizzled 7 in complex with heterotrimeric Gs. *Cell Res*. (2021) doi:10.1038/s41422-021-00525-6.
33. Yang, S. *et al*. Crystal structure of the Frizzled 4 receptor in a ligand-free state. *Nature* **560**, 666–670 (2018).
34. Eastman, P. *et al*. OpenMM 7: Rapid development of high performance algorithms for molecular dynamics. *PLoS Comput. Biol*. **13**, 1–17 (2017).
35. Zhang, Y. & Skolnick, J. Scoring function for automated assessment of protein structure template quality. *Proteins Struct. Funct. Genet*. **57**, 702–710 (2004).
36. Xu, J. & Zhang, Y. How significant is a protein structure similarity with TM-score = 0.5? *Bioinformatics* **26**, 889–895 (2010).
37. Zhang, Y. & Skolnick, J. TM-align: A protein structure alignment algorithm based on the TM-score. *Nucleic Acids Res*. **33**, 2302–2309 (2005).
38. Bouatta, N., Sorger, P. & AlQuraishi, M. Protein structure prediction by AlphaFold2: Are attention and symmetries all you need? *Acta Crystallogr. Sect. D Struct. Biol*. **77**, 982–991 (2021).
39. Saldaño, T. *et al*. Impact of protein conformational diversity on AlphaFold predictions. *bioRxiv* 1–20 (2021).
40. Mariani, V., Biasini, M., Barbato, A. & Schwede, T. IDDT: A local superposition-free score for comparing protein structures and models using distance difference tests. *Bioinformatics* **29**, 2722–2728 (2013).
41. Zheng, Y. *et al*. Structure of CC Chemokine Receptor 5 with a Potent Chemokine Antagonist Reveals Mechanisms of Chemokine Recognition and Molecular Mimicry by

HIV. *Immunity* **46**, 1005-1017.e5 (2017).
42. Zhang, H. *et al*. Structural basis for chemokine recognition and receptor activation of chemokine receptor CCR5. *Nat. Commun.* **12**, 1–12 (2021).
43. Coleman, J. A., Green, E. M. & Gouaux, E. X-ray structures and mechanism of the human serotonin transporter. *Nature* **532**, 334–339 (2016).
44. Coleman, J. A. *et al*. Serotonin transporter–ibogaine complexes illuminate mechanisms of inhibition and transport. *Nature* **569**, 141–145 (2019).
45. Tanaka, Y. *et al*. Structural basis for the drug extrusion mechanism by a MATE multidrug transporter. *Nature* **496**, 247–251 (2013).
46. Zakrzewska, S. *et al*. Inward-facing conformation of a multidrug resistance MATE family transporter. *Proc. Natl. Acad. Sci. U. S. A.* **116**, 12275–12284 (2019).
47. Kuk, A. C. Y., Hao, A., Guan, Z. & Lee, S. Y. Visualizing conformation transitions of the Lipid II flippase MurJ. *Nat. Commun.* **10**, (2019).
48. Kuk, A. C. Y., Mashalidis, E. H. & Lee, S.-Y. Crystal structure of the MOP flippase MurJ in an inward-facing conformation. *Nat. Struct. Mol. Biol.* **24**, 171–176 (2017).
49. Claxton, D. P., Jagessar, K. L. & Mchaourab, H. S. Principles of Alternating Access in Multidrug and Toxin Extrusion (MATE) Transporters. *J. Mol. Biol.* **433**, 166959 (2021).
50. Ollikainen, N., Smith, C. A., Fraser, J. S. & Kortemme, T. *Flexible backbone sampling methods to model and design protein alternative conformations. Methods in Enzymology* vol. 523 (Elsevier Inc., 2013).
51. Crawley, S. W. *et al*. Autophosphorylation activates Dictyostelium myosin II heavy chain kinase A by providing a ligand for an allosteric binding site in the α-kinase domain. *J. Biol. Chem.* **286**, 2607–2616 (2011).
52. Ping, Y. Q. *et al*. *Structures of the glucocorticoid-bound adhesion receptor GPR97–Go complex. Nature* vol. 589 (Springer US, 2021).
53. Pak, M. A. *et al*. Using AlphaFold to predict the impact of single mutations on protein stability and function. *bioRxiv* 2021.09.19.460937 (2021).
54. Akdel, M. *et al*. A structural biology community assessment of AlphaFold 2 applications. *bioRxiv* 2021.09.26.461876 (2021).
55. Mirdita, M., Ovchinnikov, S. & Steinegger, M. ColabFold - Making protein folding accessible to all. *bioRxiv* 2021.08.15.456425 (2021).
56. Steinegger, M. & Söding, J. MMseqs2 enables sensitive protein sequence searching for the analysis of massive data sets. *Nat. Biotechnol.* **35**, 1026–1028 (2017).
57. Mirdita, M., Steinegger, M. & Söding, J. MMseqs2 desktop and local web server app for fast, interactive sequence searches. *Bioinformatics* **35**, 2856–2858 (2019).
58. Roe, D. R. & Cheatham, T. E. PTRAJ and CPPTRAJ: Software for processing and analysis of molecular dynamics trajectory data. *J. Chem. Theory Comput.* **9**, 3084–3095 (2013).
59. Goddard, T. D. *et al*. UCSF ChimeraX: Meeting modern challenges in visualization and analysis. *Protein Sci.* **27**, 14–25 (2018).
60. Valero-Mora, P. M. *ggplot2: Elegant Graphics for Data Analysis . Journal of Statistical Software* vol. 35 (2010).

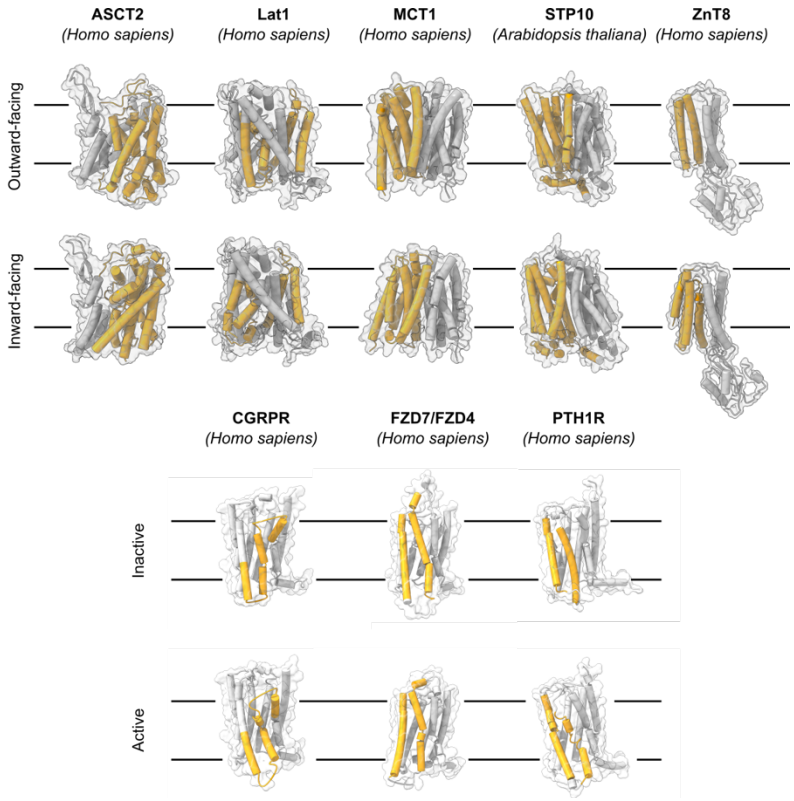

Figure S1. Structures of benchmark proteins used in this study. Top: Transporters. **Bottom:** GPCRs.

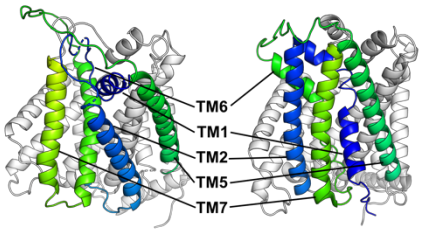

Figure S2. Example of a misfolded model of Lat1 generated using shallow MSAs. The experimental structure in an OF conformation is shown on the right. Regions that overlap are shown in white for clarity.

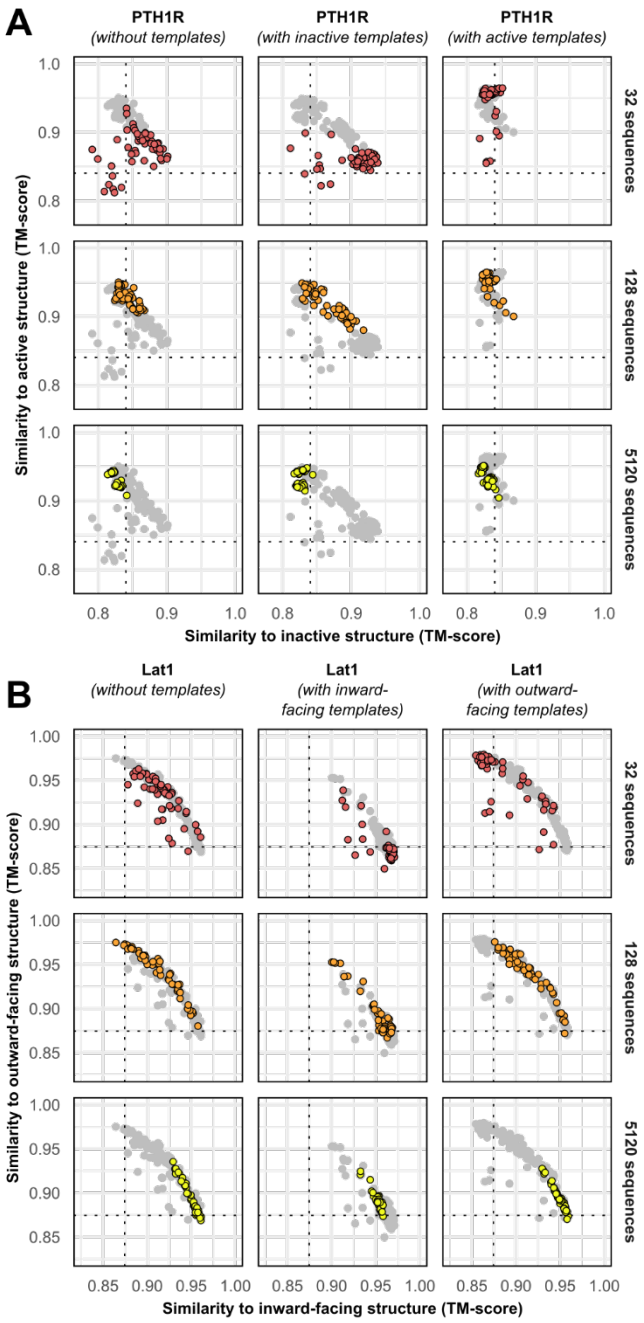

Figure S3. Templates contribute to conformational sampling only when shallow MSAs are provided. **(A)** PTH1R. **(B)** Lat1.

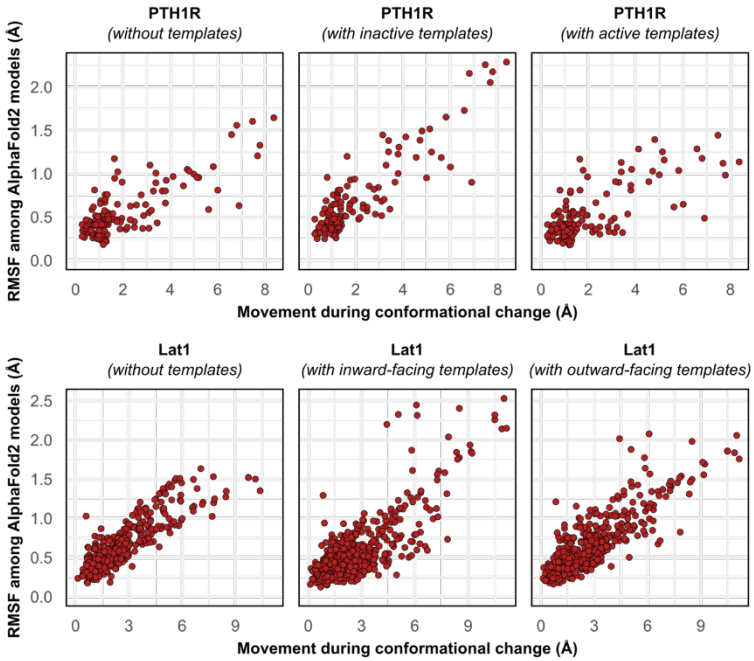

Figure S4. Comparison between each residue's RMSD in the two experimental structures of PTH1R and Lat1 and their RMSF values among AF2 models generated with templates.

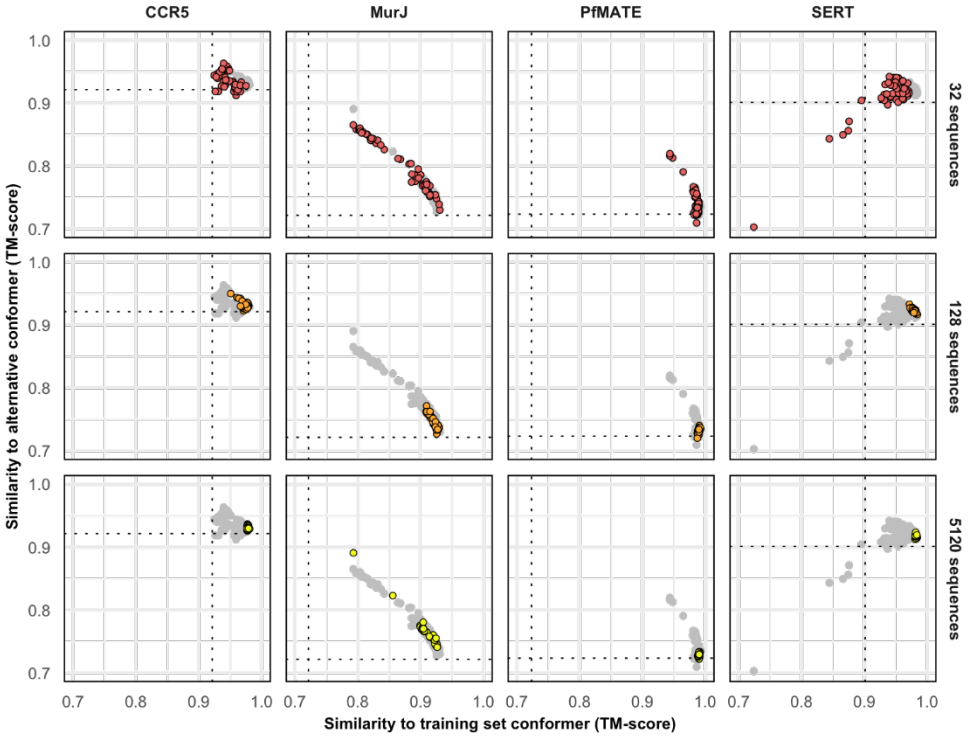

Figure S5. Protein targets with one conformation in the training set cannot be predicted in the alternative conformation.

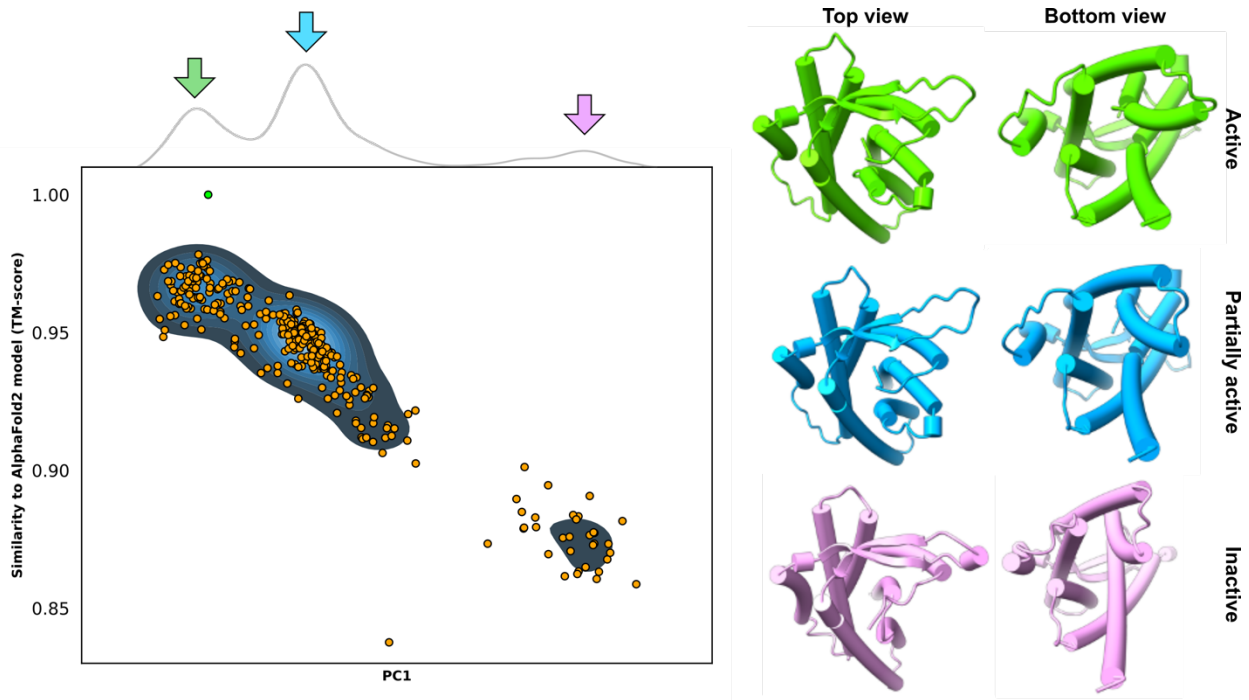

Figure S6. Example predictions of the adhesion GPCR GPR114/AGRG5. Top: Kernel density estimate of the first principal component (PC1) following PCA on all AF2 models. **Bottom:** Comparison of PC1 and TM-score values; alignments were measured from the AF2 database model, which is indicated by the green dot. **Right:** Models extracted from the cluster centers appear to adopt three distinct conformations.

Table S1. Protein targets used in this study that were absent from the AF2 training set.

Protein	Organism	Outward-facing/active	Inward-facing/inactive
CGRP	*Homo sapiens*	6UVA[28]	7KNT[29]
FZD7/FZD4	*Homo sapiens*	7EVW[32]	6BD4[33]
PTH1R	*Homo sapiens*	6NBF[31]	6FJ3[30]
ASCT2	*Homo sapiens*	7BCQ[26]	6RVX[27]
Lat1	*Homo sapiens*	7DSQ[22]	6IRS[21]
MCT1	*Homo sapiens*	7CKR[24]	7DA5[24]
STP10	*Arabidopsis thaliana*	7AAQ[25]	7AAR[25]
ZnT8	*Homo sapiens*	6XPF (chain A)[23]	6XPF (chain B)[23]

Table S2. Protein targets used in this study with one conformation present in the AF2 training set.

Protein	Organism	Training set PDB	Alternative PDB
CCR5	*Homo sapiens*	5UIW[41]	7F1Q[42]
MurJ	*Escherichia coli*	5T77[48]	6NC9[47]
PfMATE	*Pyrococcus furiosus*	3VVN[45]	6FHZ[46]
SERT	*Homo sapiens*	5I6X[43]	6DZZ[44]